Penerbit Akademia Baru

Journal of Advanced Research in Experimental Fluid Mechanics and Heat Transfer

Journal homepage:
http://www.akademiabaru.com/submit/index.php/arefmht
ISSN: 2756-8202

A Comparative Study of Cambering and Vortex Generators for Flow Separation and Turbulence Characteristics Control on a NACA 0009 Airfoil

Abdeen Osman[1], Khaled El Haj Youssef[1], Joaquin Pagaling[1], Sharul Sham Dol[1,*], Kamarul Ahmad[2], Mohammad Alkhedher[1]

[1] Mechanical and Industrial Engineering Department, Abu Dhabi University, Abu Dhabi, United Arab Emirates
[2] Department of Aerospace Engineering, Universiti Putra Malaysia, 4300 Serdang Selangor, Malaysia

ARTICLE INFO

Article history:
Received 5 May 2025
Received in revised form 18 August 2025
Accepted 29 September 2025
Available online 9 October 2025

Keywords:
Boundary Layer Control; Flow Separation; Morphing Camber; Turbulent Kinetic Energy; Vortex Generator

ABSTRACT

This study examines the aerodynamic performance of the NACA 0009 airfoil under various flow control strategies, with a focus on the effects of cambering and vortex generators (VGs) at different angles of attack (AOA). Computational fluid dynamics (CFD) simulations were conducted to analyze velocity distributions, turbulent kinetic energy (TKE), and flow separation characteristics. The results demonstrated that at an AOA of 17°, uncambered without VGs, TKE peaked at 170 m^2/s^2, indicating severe flow separation and wake turbulence. When VGs and cambering were applied, TKE reduced to 140 m^2/s^2, highlighting improved flow stability and delayed separation. At AOA 15° with VGs, TKE remained below 8 m^2/s^2, confirming effective boundary layer control, while in the cambered case without VGs, TKE reached 100 m^2/s^2, indicating that cambering alone could not fully prevent separation. The study underscores that VGs are more effective in high-AOA conditions, while cambering optimizes pressure distribution but requires additional flow control mechanisms for enhanced performance. Optimization strategies, including the Taguchi method and machine learning-based adaptive VG configurations, are recommended for future aerodynamic improvements.

1. Introduction

1.1 Literature Review

The NACA 0009 airfoil, having a symmetrical profile with a maximum thickness of 9% of its chord length, is widely used in aerodynamic applications such as rotorcraft, propellers, and control surfaces. This symmetrical configuration plays a pivotal role in applications where minimal pitching moments and predictable aerodynamic behaviour are essential. However, like all airfoils, the NACA 0009 is subject to turbulence and flow separation, influencing its aerodynamic performance under several conditions. At low angles of attack, the airflow remains largely attached, ensuring stable and efficient

* *Corresponding author.*
E-mail address: sharulshambin.dol@adu.ac.ae (Sharul Sham Dol)

https://doi.org/10.37934/arefmht.22.1.832

lift generation. As the angle of attack (AOA) increases, flow separation becomes a significant concern [1,2]. The issue becomes even more significant in higher Reynolds numbers, where adverse pressure gradients cause the boundary layer to detach from the surface [3]. This, consequently, leads to increased drag and unsteady aerodynamic forces, impacting structural integrity and efficiency in various wind turbine and aerial vehicle applications. Studies have shown that the NACA 0009 exhibits a relatively early transition to turbulence, particularly in unsteady flow conditions. This characteristic causes vortex shedding and oscillatory aerodynamic loads [4]. Efforts to mitigate these effects include the use of leading-edge modifications, active flow control strategies, and bioinspired design features aimed at delaying separation and reducing turbulence-related instabilities.

Technical innovation has always been modeled after nature, particularly in the field of aerodynamics. Through studying bats, birds, and even marine creatures like humpback whales, researchers have discovered design ideas that significantly enhance the performance of airfoils and wings [5–8]. For example, the development of serrated trailing edges for reducing aerodynamic noise in wind turbines and airplanes was inspired by the peaceful flying of owls [9]. Similar to this, advancements in airfoils that minimize stall, boost lift, and better flow separation control have been influenced by the cutting-edge tubercles seen on humpback whale flippers. These biomimetic modifications improve efficiency by changing local airflow dynamics, lowering drag, and increasing lift-to-drag ratios [10]. In micro air vehicles and drones, flexible, morphing wings fashioned after bird flight provide improved mobility and flexibility in turbulent aerodynamic environments [11]. Furthermore, advances in computational fluid dynamics (CFD) and materials science have allowed for the accurate replication of these biological traits, paving the path for more efficient and adaptable solutions that ensure occupational and environmental safety [12]. As the aerospace industry explores sustainable solutions, bioinspired engineering continues to affect the future of flying by providing unique techniques to improving performance while reducing energy consumption and environmental impact.

Morphing camber significantly impacts turbulence characteristics, with different impacts depending on application and design. Periodic trailing-edge modifications in airfoils have been demonstrated to transform wake behaviour from chaotic Kelvin-Helmholtz shedding to regulated or reversed Von-Karman shedding, providing forward thrust under specified deflection and frequency circumstances [13]. Continuous camber morphing smooths turbulence and velocity distributions, particularly at low deflection angles, but large deflections increase drag and wake instability [14]. In ground-effect operations, morphing camber reduces turbulence near the trailing edge, improving lift-to-drag ratios even in constrained proximity to the ground [15]. For micro aerial vehicles, precise camber adjustments delay flow separation and enhance aerodynamic performance, though excessive changes can amplify drag [16]. Nature-inspired designs, like spanwise morphing modeled on avian wings, suppress turbulence and create smoother wakes by delaying flow separation, improving glide efficiency [17]. Morphing camber systems are used in sophisticated aircraft to improve wake characteristics for subsonic and supersonic regimes, manage turbulence, and reduce drag across a wide speed range. These developments demonstrate morphing camber's capacity to change wake structures, manage turbulence, and improve efficiency across a wide range of aerodynamic circumstances [18,19].

Vortex Generators (VGs), which are passive flow control devices, are commonly employed in aerodynamic applications to reduce the effects of flow separation and enhance boundary layer stability by eliminating stall [20]. VGs, which are often added to the surface in arrays and inclined at specific angles to the freestream, generate streamwise vortices that actively energize the near-wall region by transferring high-momentum fluid from the outer flow into the boundary layer. However, this momentum exchange makes the boundary layer more resilient to separation, particularly in

regions with adverse pressure gradients [21–23]. Since VGs maintain flow attachment over larger surface extents, they enhance the lift characteristics and lower pressure drag over the surface. Usually, they are found in these specific applications, such as wind turbine blades, airplane wings, and high-performance vehicle aerodynamics, due to the importance of the boundary layer attachment to the surface [24–26]. Usually, the VGs have characteristics that determine their effectiveness, including size, shape, spacing, and orientation relative to the direction of local flow [27].

Two distinct approaches may be used to examine the effects of morphing cambering and vortex VGs on airfoil aerodynamics: one looks at the boundary layer itself, while the other looks at the external flow characteristics outside of the boundary layer. It is anticipated that the addition of VGs will enhance momentum mixing inside the boundary layer by increasing turbulence. By energizing low-momentum fluid close to the surface, this enhanced turbulence can postpone flow separation and guarantee that the flow stays linked for a greater distance along the airfoil. Likewise, by dynamically changing the form of the airfoil, morphing cambering may improve the pressure distribution and minimize adverse pressure gradients that usually lead to separation. More efficient boundary layer management is made possible by morphing cambering, which actively alters the aerodynamic surface, especially at different AOAs. As an alternative, the external flow beyond the boundary layer may be examined to assess the impact of VGs and morphing cambering. A well-designed system should ideally maintain efficiency and minimize drag by ensuring that the exterior flow is mostly laminar with few disruptions. This dual viewpoint, which focuses on exterior laminarity and boundary layer turbulence, provides a comprehensive framework for evaluating the improvement in aerodynamic properties.

1.2 Research Gap and Study Scope

Morphing camber mechanisms and VGs have gained increasing traction in several aerodynamic applications for their potential to delay leading-edge flow separation. The NACA 0009 airfoil remains a commonly used reference in aerodynamic studies due to its symmetric profile and suitability for controlled investigations. However, there remains a significant lack of quantitative turbulence characterization and effect on flow separation for both morphing cambers and VGs individually. Additionally, there is a near-complete absence of comparative or combined studies examining their synergistic effects. This study addresses this gap by investigating the turbulence behaviour and flow control performance of each strategy individually and combined, focusing on leading-edge separation dynamics and flow control interaction. This study quantitative and statistical analysis of flow structures over the morphing NACA 0009 with VGs near the leading edge offers the following key contributions: (1) evaluating turbulence characteristics and velocity distribution across the airfoil to develop a deeper understanding of the flow separation phenomena associated with morphing cambers and VGs; (2) analyzing velocity fluctuations to quantify turbulence generation, shedding light on unsteady aerodynamic effects introduced by camber variation and addition of VGs; and (3) assessing the turbulent kinetic energy budgets to examine localized shear production across the airfoil surface. This research offers valuable insights into the complex turbulence behaviour of morphing camber airfoils and VGs through a structured, data-driven approach, providing a critical reference for future aerodynamic optimization and performance enhancements.

This study is organized into five sections, covering the turbulence and flow separation analysis of the morphing camber of the NACA0009 airfoil. The rest of this paper is as follows: Section 2 presents the physical modeling of the study, including continuity, momentum, and turbulence characterization. Section 3 introduces the methodology followed in this study, covering the CFD

setup, experimental protocol, and apparatus. Section 4 is the core section of this paper, with all the results and discussions associated with the flow separation, velocity profiles, and turbulence generation characterization. Finally, Section 5 summarizes this study's main conclusions, key contributions, and future recommendations.

2. Physical Model of the Study

2.1 The continuity and Momentum Equations

Using the k-ω SST turbulence model, which offers a better forecast of boundary layer effects and flow separation under adverse pressure gradients [28,29], the aerodynamic behaviour of the morphing NACA 0009 airfoil is examined. Using a blending function, this model efficiently switches between k-ε (for free-stream turbulence) and k-ω (for near-wall effects), guaranteeing precise depiction of turbulent viscosity and eddy formation. The transport and dissipation of turbulent structures are captured by the governing equations for turbulent kinetic energy (k) and specific dissipation rate (ω). While the ω-equation considers energy dissipation and turbulence scale variation, the k-equation describes the development of turbulent energy as a result of shear generation and diffusion. The k-equation describes the evolution of turbulent energy due to shear production and diffusion, while the ω-equation accounts for energy dissipation and turbulence scale variation. Together, they determine turbulence intensity and its impact on flow structures over the airfoil. These equations are solved using a pressure-based solver in a transient simulation framework, with second-order discretization applied to ensure numerical stability. The eddy viscosity (ν_t) is computed as the ratio of k to ω, providing insight into local turbulence variations across the morphing airfoil, particularly at regions of rapid camber change where shear layers form.

The governing equations for the unsteady, incompressible turbulent flow are based on the Reynolds-Averaged Navier-Stokes (RANS) formulation. The continuity equation is:

$$\frac{\partial u_i}{\partial x_i} = 0 \tag{1}$$

where u_i is the velocity component in the xi direction. The momentum equation, incorporating Reynolds stress tensor, is:

$$\rho\left(\frac{\partial u_i}{\partial t} + u_j\frac{\partial u_i}{\partial x_j}\right) = -\frac{\partial P}{\partial x_i} + \frac{\partial}{\partial x_j}\left[\mu\left(\frac{\partial u_i}{\partial x_j} + \frac{\partial u_j}{\partial x_i}\right)\right] - \frac{\partial \rho\overline{u_i'u_j'}}{\partial x_j} \tag{2}$$

2.2 Turbulence Quantification

Based on the surface and flow characteristics, and to achieve a Y+ value of 1 [30], the estimated wall distance required for accurate resolution of the boundary layer characteristics and a detailed physical analysis of the boundary itself is 7.7e-3 mm as shown in Table. 1. This number reflects the maximum element size that should be utilized in meshing near the airfoil's surface to capture viscous sublayer effects effectively. However, a greater element size was chosen to guarantee a balance between accuracy and computational viability because of the high processing needs associated with such an extremely fine mesh. To get a thorough knowledge of the aerodynamic impacts of VGs and morphing cambering, we decided to investigate the exterior flow characteristics rather than concentrating on resolving the boundary layer at such a tiny scale. We can evaluate the wider effects of these changes on separation control, lift-to-drag optimization, and aerodynamic efficiency by examining the external flow. This approach allows for meaningful insights into the overall flow

behaviour while significantly reducing computational costs, making the study more practical without compromising the core objectives of the analysis.

Table 1
Estimated wall distance based on Y+ values

Parameters	Values
Free Stream Velocity (m/s)	**44.32**
Density kg/m3	**1.225**
Dynamic Viscosity (kg/ms)	**1.82e-2**
Boundary Layer Length (m)	**0.3105**
Desired Y+ Value	**1**
Estimated Wall Distance m	**7.7e-6**

The behaviour of fluctuation parameters may be explained by using the Reynolds decomposition method on the Navier-Stokes equations, followed by a sequence of modifications to generate the kinetic energy budget, which characterizes the energy of turbulence. To study the transfer of turbulence energy, there are two kinetic energy budgets: one for the mean flow and one for the turbulent flow. This is because the kinetic energy budget gives information about how the turbulence spreads and dissipates after it is generated from the mean flow. The kinetic energy budget of mean flow may be expressed as:

$$\frac{D}{Dt}\left(\frac{1}{2}U_i^2\right) = \frac{\partial}{\partial x_j}\left(-\frac{PU_j}{\rho_o} + 2\nu U_i E_{ij} - \overline{u_i' u_j'} U_i\right) - 2\nu E_{ij}E_{ij} + \overline{u_i' u_j'}\,\frac{\partial U_i}{\partial x_j} - \frac{g}{\rho_o}\bar{\rho}\, U_3 \tag{3}$$

$$\frac{D}{Dt}\left(\overline{\frac{1}{2}u_i'^2}\right) = -\frac{\partial}{\partial x_j}\left(\overline{\frac{pu_j'}{\rho_o}} - 2\nu\overline{u_i' e_j} + \overline{\frac{1}{2}u_i' u_i' u_j'} U_i\right) - 2\nu\overline{e_{ij}e_{ij}} - \overline{u_i' u_j'}\,\frac{\partial U_i}{\partial x_j} + g\alpha\overline{\omega T'} \tag{4}$$

The kinetic energy budget equation offers an outline for comprehending how turbulence energy is transferred, generated, and dissipated in the flow. The performance of bioinspired airfoil alterations may be assessed by examining each component in this equation to determine how the turbulence changes spatially and dynamically under different flow conditions. The production term, $\overline{u_i' u_j'}\,\frac{\partial U_i}{\partial x_j}$, which denotes the energy transfer from the mean flow to the turbulent flow, is very significant. This part, which is usually positive in the turbulent energy budget, denotes the transfer of energy from the mean flow's structured motion into the chaotic turbulent motion. We can pinpoint the areas of the flow where turbulence is being actively produced by localizing and measuring this term. This entails comprehending how adjustments, such shifts in camber or AOA, impact the creation of turbulence close to crucial areas like the wake, leading edge, and trailing edge of the airfoil. The dissipation term, $2\nu\overline{e_{ij}e_{ij}}$, represents the loss of turbulence energy due to viscous effects. This term becomes significant in regions where small-scale turbulent structures dominate, such as within boundary layers or in separated flows. Comparing the dissipation across different airfoil configurations provides insight into how the modifications influence energy losses.

The localized production and dissipation terms in the flow field may be seen and measured with CFD simulations and the corresponding post-processing. We can identify areas of highest turbulence formation by mapping these values at various cambers and angles of attack. For example, a bioinspired design that postpones flow separation may produce less turbulence close to the trailing edge, which would lessen drag and wake turbulence. We can also assess how well the airfoil mitigates

adverse flow effects by looking at the size of the production term in high-turbulence areas. The kinetic energy budget eventually helps in assessing if an airfoil alteration succeeds in enhancing flow stability and lowering turbulence, particularly at higher angles of attack where traditional designs might not work.

To assess the turbulent momentum transfer and flow behaviour at high angles of attack, the Reynolds stresses for the bioinspired airfoils were examined. The Reynolds averaged Navier-Stokes equation may be expressed as in equation (5) where the Reynolds stress is the part of the overall stress tensor in a fluid that is derived from the averaging process across it. The time-averaged products of varying velocity components, normalized by the square of the freestream velocity, were used to calculate the Reynolds stresses. Regions of substantial turbulent energy in the flow were identified using the normalized streamwise stress, which is the square of the fluctuating streamwise velocity divided by the freestream velocity squared, or ($\frac{\overline{u_i'^2}}{U^2}$). To evaluate the impact of turbulence in these directions, the wall-normal and spanwise Reynolds stresses, or ($\frac{\overline{v_i'^2}}{U^2}$ and $\frac{\overline{w_i'^2}}{U^2}$), were also computed. To measure the momentum transfer between the streamwise and wall-normal directions—a crucial component in comprehending turbulent energy production—the turbulent shear stress, sads, was also examined. The analysis was conducted at key regions along the airfoil and its wake, including the leading edge, trailing edge, and downstream wake at distances of one to two chord lengths. The leading edge was examined to capture the initiation of boundary layer development and shear stress formation, while the trailing edge was studied for its role in vortex generation and turbulence amplification. In the wake, the Reynolds stresses highlighted the turbulent fluctuations dominating this region, providing insights into the effect of airfoil modifications on wake dynamics.

$$\frac{\partial \overline{u_i}}{\partial t} + \overline{u_j}\frac{\partial \overline{u_i}}{\partial x_j} = \frac{1}{\rho}\frac{\partial}{\partial x_j}\left(\overline{\tau_{ij}} - \overline{\rho u_i' u_j'}\right) \tag{5}$$

3. Methodology

3.1 Simulation Setup and Post-processing

The analysis was carried out with a morphing airfoil based on the NACA 0009 profile with integrated VG. The 3D geometry was initially created in Fusion 360 and then exported to ANSYS DesignModeler. To approximate trailing-edge deformation, the morphing profile uses a flexible camber that is parametrically controlled. VGs were inserted at the leading edge and positioned in a streamwise direction to create controlled turbulence in the boundary layer. A fluid domain was created using the "Enclosure" tool to imitate a wind tunnel environment. A rectangular computational zone surrounded the airfoil, with sufficient space upstream, downstream, and normal to the chord to minimize border interference effects. To adequately describe boundary conditions, the final geometry contained individual named choices for the inlet, outlet, airfoil walls, and domain walls. The simulation setup is shown in Fig. 1 where the geometry is shown in (a) and the meshing is shown in (b).

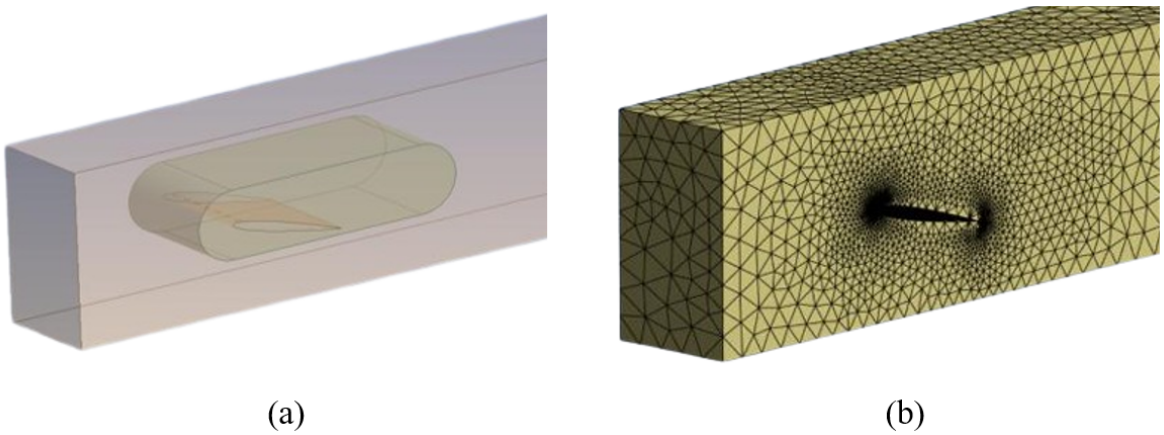

Fig. 1. Simulation setup demonstrating: (a) the airfoil and (b) the meshing around it.

Meshing was carried out via ANSYS Meshing, with a focus on resolving boundary layer and VG-induced shear zones. A linear tetrahedral mesh with roughly 900,500 elements was created using curvature-based refinement and edge scaling near sharp features. A Bias Factor of 150 was used for further refinement around the VGs surfaces and trailing edge morphing zones, ensuring exact resolution of fine-scale flow dynamics. Inflation layers were introduced, with a maximum of 5 layers and a growth rate of 1.15, to enable realistic near-wall simulation. Mesh quality metrics were assessed using skewness, and mesh defeaturing was allowed with a minimum curvature size of 1.2 mm. The total mesh was tested for convergence and continuity of wall-adjacent parts. The meshing characteristics are listed in Table 2.

Table 1
Summary of the meshing and element size parameters

Parameter	Value
Element Size (mm)	30
Max Element Size (mm)	50
Growth Rate	1.15
Inflation Layers	5
Mesh Defeaturing	Enabled
Skewness Metric	Medium
Curvature Normal Angle	16.5°
Min. Curvature Size (mm)	1.2

CFD simulations were conducted using ANSYS Fluent in a transient flow regime to accurately capture unsteady vortex interactions and flow separation phenomena. The pressure-based solver was selected for its stability in low-Mach subsonic flows, and second-order upwind discretization was applied to improve numerical accuracy across spatial gradients. The SST k–ω turbulence model was used due to its superior performance in resolving boundary layer behaviour under adverse pressure gradients—especially near separation zones induced by high angles of attack and morphing deformations. The simulation assumed an incompressible flow at a freestream velocity of 44.32 m/s,

corresponding to a Reynolds number of approximately 970,000. This range was selected to mimic typical operating conditions of small unmanned aerial vehicles (UAVs) and wind tunnel test scenarios. Simulations were carried out over a range of angles of attack (0°–25°) to evaluate lift, drag, and flow stability transitions. The simulation parameters and boundary conditions are listed in Table 3.

Table 2
Summary of the study's boundary conditions and analysis setup

Parameter	Value
Reynolds Number	~970,000
Freestream Velocity (m/s)	44.32
Turbulence Model	SST k–ω (2-equation)
Time-Stepping	Transient
Time Step Size (s)	0.01
Number of Time Steps	5000
Max Iterations per Time Step	200
Inlet Boundary Condition	Velocity Inlet
Outlet Boundary Condition	Pressure Outlet (0 Pa)
Turbulent Intensity (Backflow)	3.5%
Viscosity Ratio (Backflow)	7
Operating Pressure (Pa)	101325
Operating Density (kg/m³)	1.225
Solver Coupling	COUPLED
Initialization	Hybrid Initialization
Gravitational Acceleration	-9.81 m/s² (Y-axis)

Finding the velocity distribution over the airfoil surface is the most important part of this simulation as it has a direct impact on flow separation, turbulence production, and aerodynamic efficiency. The instantaneous velocity data at different positions along the airfoil was captured using a time-series extraction technique because ANSYS Fluent does not directly offer time-averaged velocity fields. This approach allows precise analysis of velocity fluctuations brought on by morphing camber, enabling a thorough evaluation of unsteady flow features. This was accomplished by extracting velocity data over time at several points on the airfoil surface, especially at areas that are prone to vortex shedding, boundary layer separation, and development. The time-averaged velocity field and instantaneous velocity variations were then calculated using statistical processing of these instantaneous velocity measurements. In comparison to direct solver outputs, this method offers a more detailed representation of the turbulent flow structures and guarantees that the effects of morphing camber on flow stability, Reynolds stresses, and kinetic energy distribution are accurately characterized for performance optimization. By analyzing these fluctuations, we quantify the degree of turbulence, shear production, and flow unsteadiness introduced by the morphing camber.

3.2 Experimental Setup and Procedure

The experimental setup, shown in Fig. 2, was designed to evaluate the aerodynamic performance of an airfoil under different geometric alterations, especially cambering and the insertion of VGS,

over a wide range of AOA. A low-speed wind tunnel was built with a fog generator, a settling chamber, a transparent test section, and an axial fan blower to assure regulated and constant airflow. The fog generator produced tracer particles, which were fed into the flow via a PVC duct system linked to a dual layer settling chamber composed of MDF panels. This chamber was built to decrease turbulence and increase flow uniformity before the test section. The test area itself was designed with an acrylic side wall for direct flow viewing and image capturing. The airfoil model, which is replaceable for different configurations, was installed horizontally within the test section to allow for controlled AOA modification.

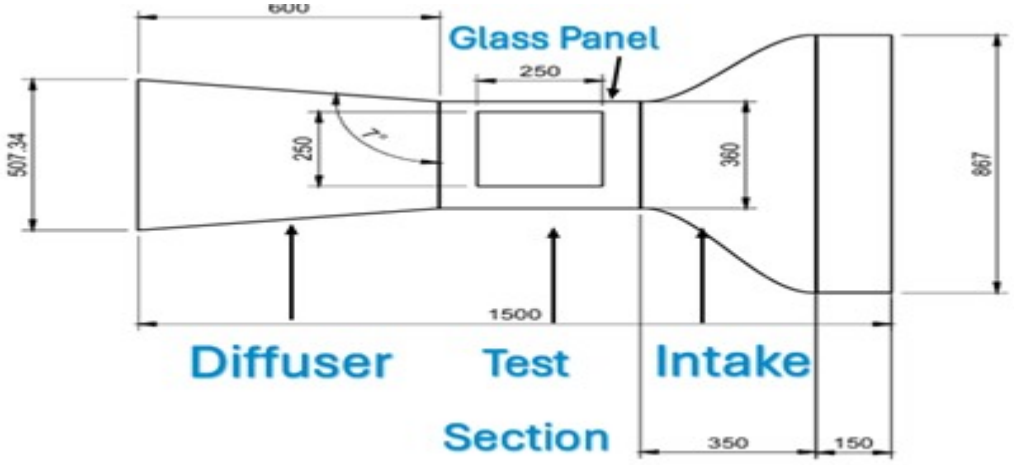

Fig. 2. A schematic of the wind tunnel where the experimental testing of the airfoil modifications and active cambering is conducted.

To examine the impact of cambering and VGS, flow visualization was performed using smoke created by the fog machine, which allowed for the observation of flow attachment, separation points, and wake characteristics. The axial fan at the exit created airflow by suction, resulting in uniform low-speed wind conditions suited for qualitative aerodynamic analysis. Each airfoil configuration was evaluated at varied AOA increments to detect performance changes, emphasizing flow separation behaviour and vortex generation. The design allowed for repeated trials under consistent flow conditions, with visual observations recorded through the glass panel for further study. Although this technique focuses on qualitative flow behaviour, it may be supplemented by pressure sensors or force-measuring tools for further quantitative confirmation in future investigations.

4. Results and Discussion

4.1 Delayed Flow Separation Characteristics

The first analysis conducted focuses on evaluating the effect of cambering and VGs on flow separation across three different AOAs: 15°, 17°, and 18°. At AOA 15°, the primary focus is on examining the impact of cambering. By dynamically altering the airfoil shape, cambering helps optimize the pressure distribution along the surface, reducing adverse pressure gradients and consequently delaying flow separation. This adjustment is particularly beneficial in improving lift generation while minimizing drag. At AOA 17°, we investigate the combined influence of both cambering and VGs. The simultaneous application of these techniques is expected to enhance flow attachment further by not only modifying the pressure gradient through cambering but also

introducing controlled turbulence through VGs. This interaction aims to energize the boundary layer, keeping it attached for longer and mitigating separation effects. Finally, at AOA 18°, we specifically analyze the effect of VGs alone. VGs function by generating streamwise vortices, increasing boundary layer mixing, and preventing premature separation, especially at higher AOAs. This analysis provides a comprehensive understanding of how each technique individually and collectively influences aerodynamic performance, offering insights into their effectiveness in delaying separation and improving lift-to-drag ratios across varying flight conditions.

4.1.1 Cambered at Angle of Attack 17 with Vortex Generators

At an AOA of 17°, the velocity contour plots show how cambering and VGs affect flow separation and the creation of a recirculation zone. The change in the flow separation position caused by the applied adjustments is among the most important findings from these figures. Without any changes, flow separation happens early close to the leading edge at x/D = 0.13 in Fig. 3 (a). A sizable recirculation zone is produced by this early separation, which is distinguished by a notable low-velocity area (blue region) where flow reversal takes place. The separation at this location suggests that the boundary layer is being prevented from remaining connected to the airfoil surface by a high unfavorable pressure gradient. As a result, the airflow over the upper surface becomes highly unstable, leading to increased pressure drag and reduced lift. On the other hand, Fig. 3 (b) shows how effectively VGs and cambering work to postpone separation and minimize the severity of recirculation. With these changes, separation is considerably delayed until x/D = 0.63 and the flow stays linked for a greater distance. Two main mechanisms are responsible for the extended attachment: (1) cambering, which modifies the pressure distribution along the airfoil to lessen the strength of the adverse pressure gradient, and (2) VGs, which increase momentum exchange and strengthen the boundary layer's resistance to separation by introducing controlled turbulence.

Aerodynamic efficiency is largely dependent on the recirculation zone's size and intensity. The recirculation zone is large and extends far downstream of the separation point in Figure (a), where separation happens early. The airfoil's total lift generation has decreased, and form drag is much increased in the high-intensity backflow area. Furthermore, the large-scale turbulent wake creation seen in (a) increases the flow field's instability and aerodynamic losses. The recirculation zone is greatly decreased in (b) by applying cambering and VGs. The boundary layer is better electrified and stays connected for a long time, as seen by the flow separation point shifting from x/D = 0.13 to x/D = 0.63. As a result, the wake zone is reduced, which raises the effective lift-to-drag ratio and decreases pressure drag. The smoother transition of velocity gradients in comparison to the unmodified instance indicates that the strength of the reversed flow is also reduced. This suggests a more steady and regulated airflow, which is essential for enhancing aerodynamic efficiency in parts like wind turbine blades, airplane wings, and high-performance automobiles.

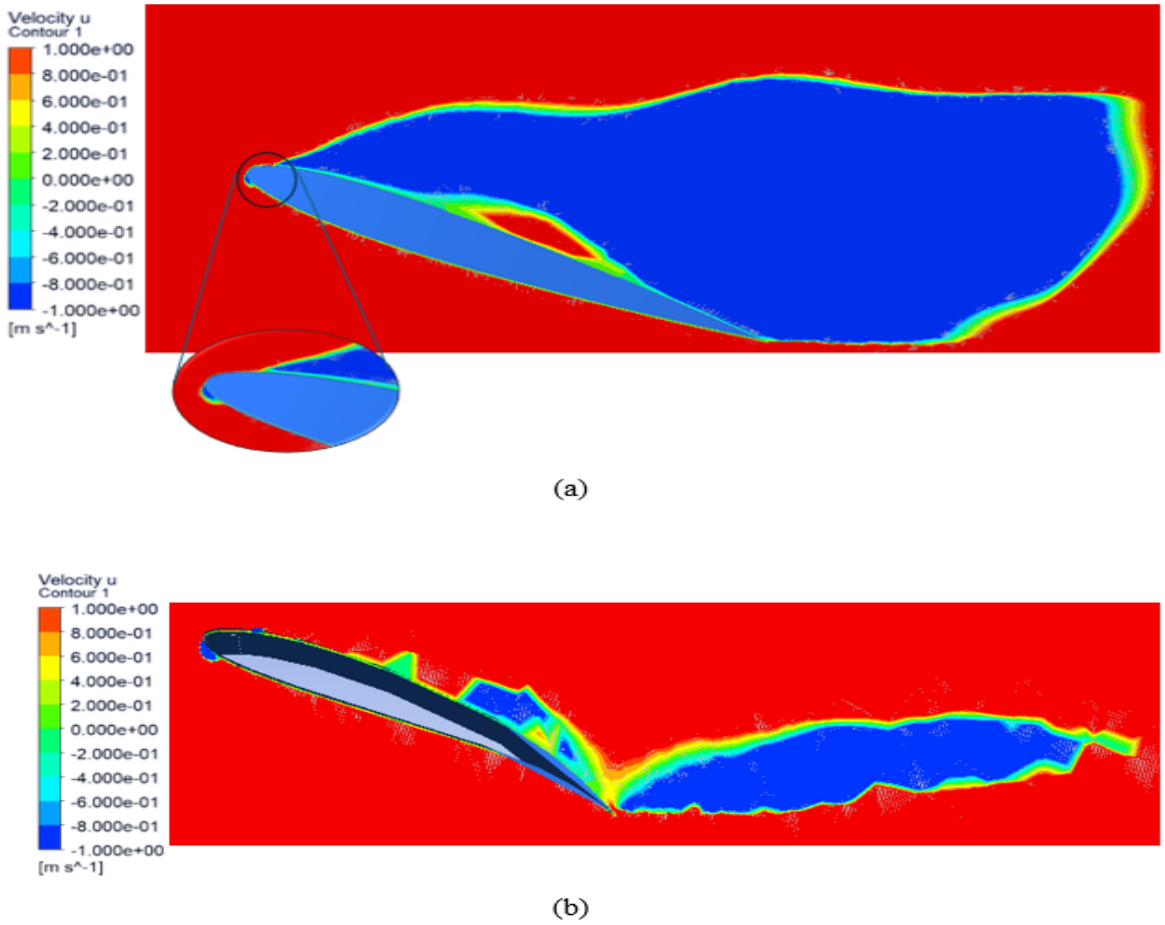

Fig. 3. Separation point for the airfoil at an AOA of 17: (a) without cambering and VGs and (b) after cambering and adding VGs near the leading edge.

4.1.2 Uncambered at Angle of Attack 18 with Vortex Generators

A new perspective on how VGs alone affect flow separation and recirculation zone development is offered by the velocity contour visualizations at AOA 18°. This scenario distinguishes the unique function of VGs in controlling boundary layer behaviour, in contrast to the AOA 17° case, when both cambering and VGs were used in tandem. Fig. 4 (a) shows that flow separation happens relatively early, at x/D = 0.12, demonstrating that the boundary layer cannot overcome the adverse pressure gradient without external intervention. A significant, low-velocity recirculation zone is created by this premature separation, greatly increasing drag and decreasing lift. In this instance, the detached shear layer creates a turbulent wake that stretches far downstream, creating a large separation bubble. The addition of VGs has an apparent impact in Fig. 4 (b), as separation delays till x/D = 0.29. This delay implies that the VGs aid in the boundary layer's transition into a more energetic, turbulent state, enhancing its resistance to the adverse pressure gradient. The main distinction between this and AOA 17° is the absence of cambering, which means that the adverse flow conditions must be accounted for by the efficiency of VGs alone. The recirculation zone is nevertheless greater than in situations when both cambering and VGs were used, even if it is smaller. This suggests that while VGs by themselves have advantages, their functionality is constrained in the absence of other geometric adjustments.

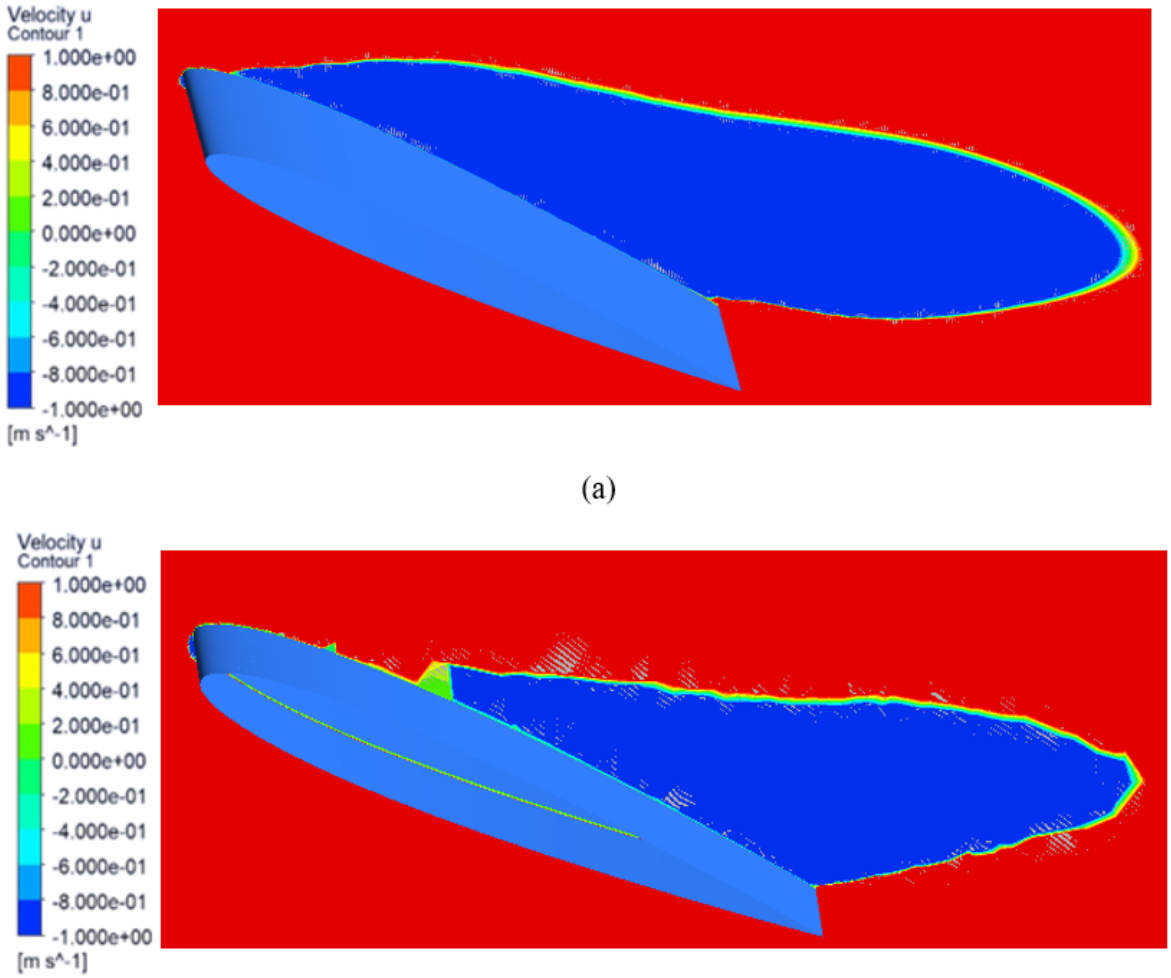

Fig. 4. Separation point at an AOA of 18: (a) without adding any modification and (b) after addition of VGs.

Beyond the delay in separation, the recirculation zone characteristics offer additional insight into the impact of VGs on the overall flow structure. In Figure (a), without VGs, the recirculation zone is large and well-defined, with a significant low-velocity region (blue zone) forming directly behind the separation point. This recirculation bubble extends far downstream, creating a wide turbulent wake that results in increased pressure drag. The recirculation zone is notably smaller and more limited in Figure (b) with VGs, suggesting that the turbulent vortices the VGs create aid in the boundary layer's ability to retain some degree of coherence prior to final separation. In comparison to the unaltered scenario, the reversed flow's intensity is lower, which means that although separation still happens, the aerodynamic losses are less. The wake's more ordered form indicates that the VGs' vortices aid in momentum redistribution and lessen the degree of flow reversal.

4.1.3 Cambered at Angle of Attack 10 with no Vortex Generators

It is evident from the velocity contour plots that cambering at a lower AOA significantly enhances aerodynamic performance. This research demonstrates that altering the airfoil shape alone is adequate to avoid separation for moderate AOA circumstances, in contrast to high-AOA instances where aggressive flow separation necessitates several flow control approaches. Without cambering,

a moderate recirculation zone forms in Fig. 5 (a) when flow separates toward the back of the airfoil at x/D = 0.65. Even though the separation is less severe than in high-AOA situations, drag and lift loss are still introduced, which lowers aerodynamic efficiency. A wake is produced, and overall resistance is increased as the boundary layer detaches, as indicated by the presence of a blue low-velocity zone close to the trailing edge. Cambering entirely eliminates flow separation and keeps the airflow fully linked over the whole airfoil surface, as seen in Fig. 5 (b). By modifying the pressure gradient along the airfoil, the cambered form keeps the boundary layer stable and energetic, avoiding early separation. In contrast to situations when VGs were required to postpone separation, cambering passively accomplishes this goal without adding further turbulence or energy losses. A narrow, streamlined boundary layer is seen in the velocity contours, demonstrating how well shape alteration preserves smooth flow attachment.

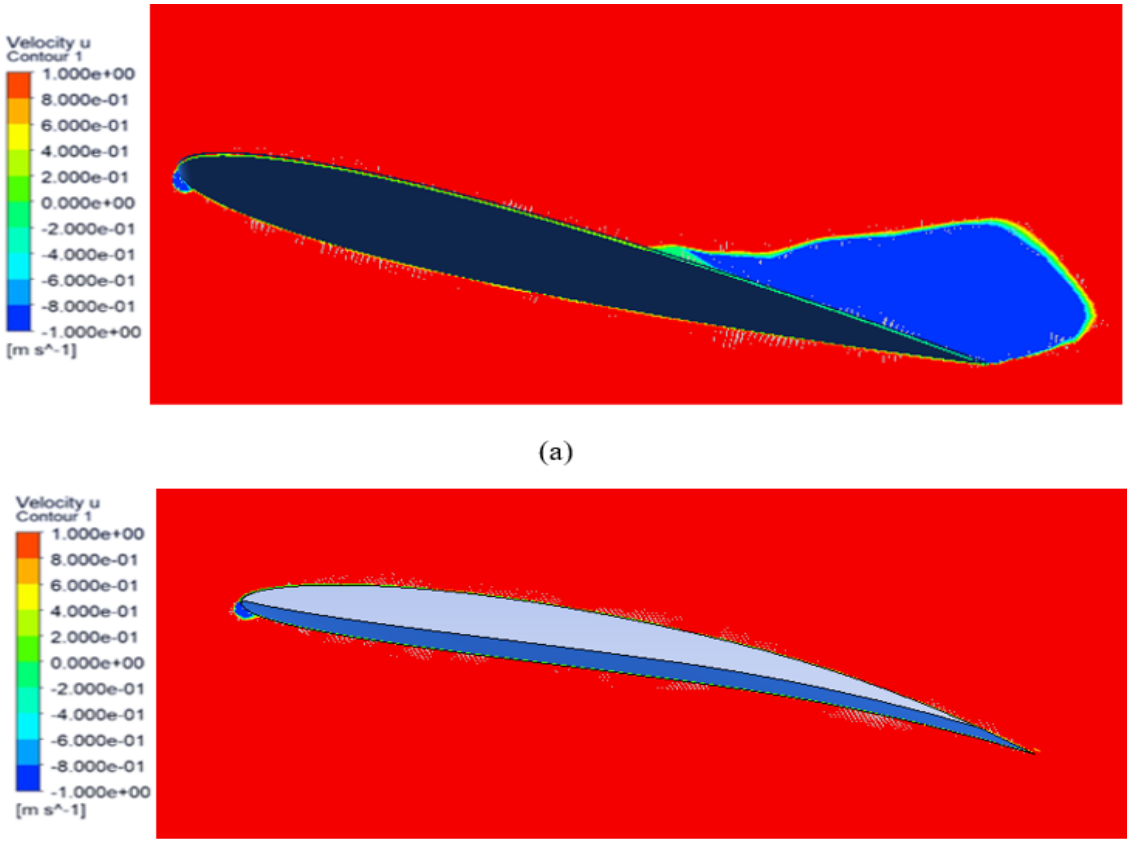

Fig. 5. Flow separation point on the airfoil at an AOA of 10: (a) without any modifications and (b) after cambering without the additions of VGs.

Because cambering offers a more effective and passive technique to maintain flow attachment without the disadvantage of higher friction drag, it is always chosen over VGs in aircraft wing designs. Although VGs successfully postpone separation, they also increase surface roughness and turbulence, which enhances skin friction drag considerably. This cumulative drag becomes a significant element influencing fuel consumption and overall flight economy on long-haul flights. Although VGs enhance boundary layer attachment, the smoother, naturally adjusted pressure distribution that cambering provides overcomes the energy cost of VGs in terms of drag. Cambered wings continue to be the favored design option because they provide greater aerodynamic efficiency

over long distances, resulting in reduced fuel consumption and increased range. While VGs can be valuable in extreme conditions, they are generally avoided in commercial aircraft wing designs unless necessary, as the focus remains on achieving the best lift-to-drag ratio with minimal energy losses.

4.1.4 Comparison Between Cambering and Vortex Generators in High Angles of Attack

At a reasonably high AOA of 15°, the velocity contour plots show the variations in flow behaviour between an airfoil with VGs is presented in Fig. 6 (a) and one with cambering (b). Since cambering efficiently redistributes pressure throughout the airfoil without adding extra friction drag, it is the recommended technique for avoiding flow separation at lower AOAs. Its efficacy is mostly restricted to minimizing separation in the vicinity of the trailing edge, where adverse pressure gradients are less pronounced. Separation is still visible in (b), but it is limited further downstream rather than at the leading edge at x/D = 0.59. However, separation tends to happen considerably earlier—closer to the leading edge—at greater AOAs, which reduces cambering's efficacy. Since cambering does not induce turbulence, it cannot energize the boundary layer enough to prevent detachment in these conditions. Instead, it simply alters the pressure distribution, which, while beneficial at low AOAs, does not provide sufficient separation control at higher angles where flow instability is more pronounced.

On the other hand, the first picture, which uses VGs, shows how these devices work better at greater AOAs. VGs cause the boundary layer to become turbulent by creating streamwise vortices close to the leading edge. This improves momentum mixing and delays premature separation. This is especially helpful since the flow is more likely to separate close to the leading edge than the trailing edge at high AOAs. VGs maintain the flow connected for a greater distance along the airfoil surface by generating early turbulence, which strengthens the boundary layer's resistance to adverse pressure gradients. In contrast to the cambered instance, the airflow is still connected much further up the chord, even with the high AOA. However, because VGs increase friction drag, they are less suitable for lower AOAs, where smooth, laminar flow is desired and separation is less forceful.

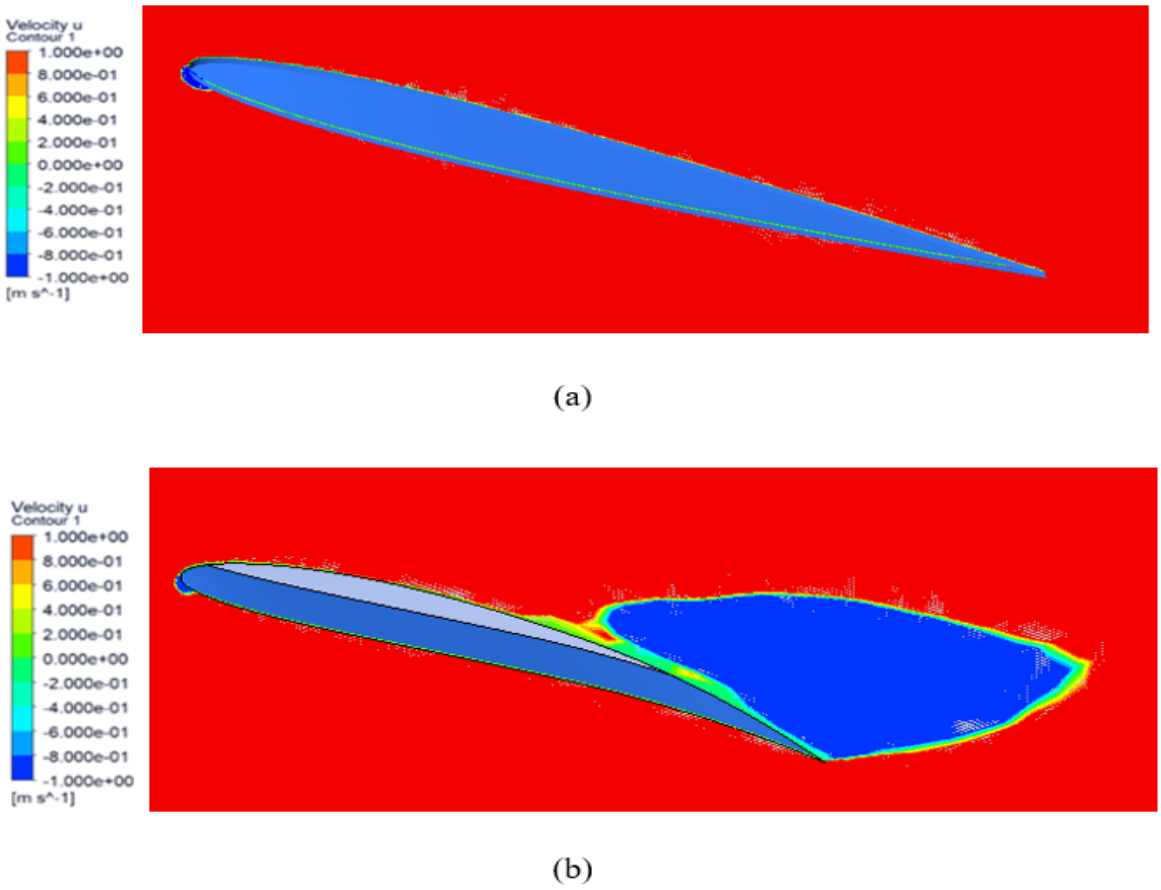

Fig. 6. Comparing the effectiveness of various airfoil modifications at an AOA of 15 where: (a) VGs are introduced near the leading edge and (B) the airfoil is cambered.

4.1.5 Experimental Validation of the Active Cambering Effects

The experimental flow visualization in a low-speed wind tunnel was utilized to confirm the CFD simulation findings by comparing velocity field behaviour and separation characteristics at various AOAs under cambered situations. As illustrated in Fig. 7 (a), at an AOA of 10°, the cambered airfoil has smooth streamlines over its top surface, with no signs of large-scale separation or flow reversal. While modest flow disruptions are seen at the trailing edge, they do not indicate complete separation and correspond well with the simulated velocity contours, which also show unbroken flow attachment and mild pressure recovery. This correlation validates the simulation's prediction of enhanced boundary layer adherence at lower angles of attack when cambering is introduced. The interaction of the camber-induced pressure gradient with the boundary layer appears to energize the flow, suppressing early separation and promoting smoother flow over the airfoil's upper surface.

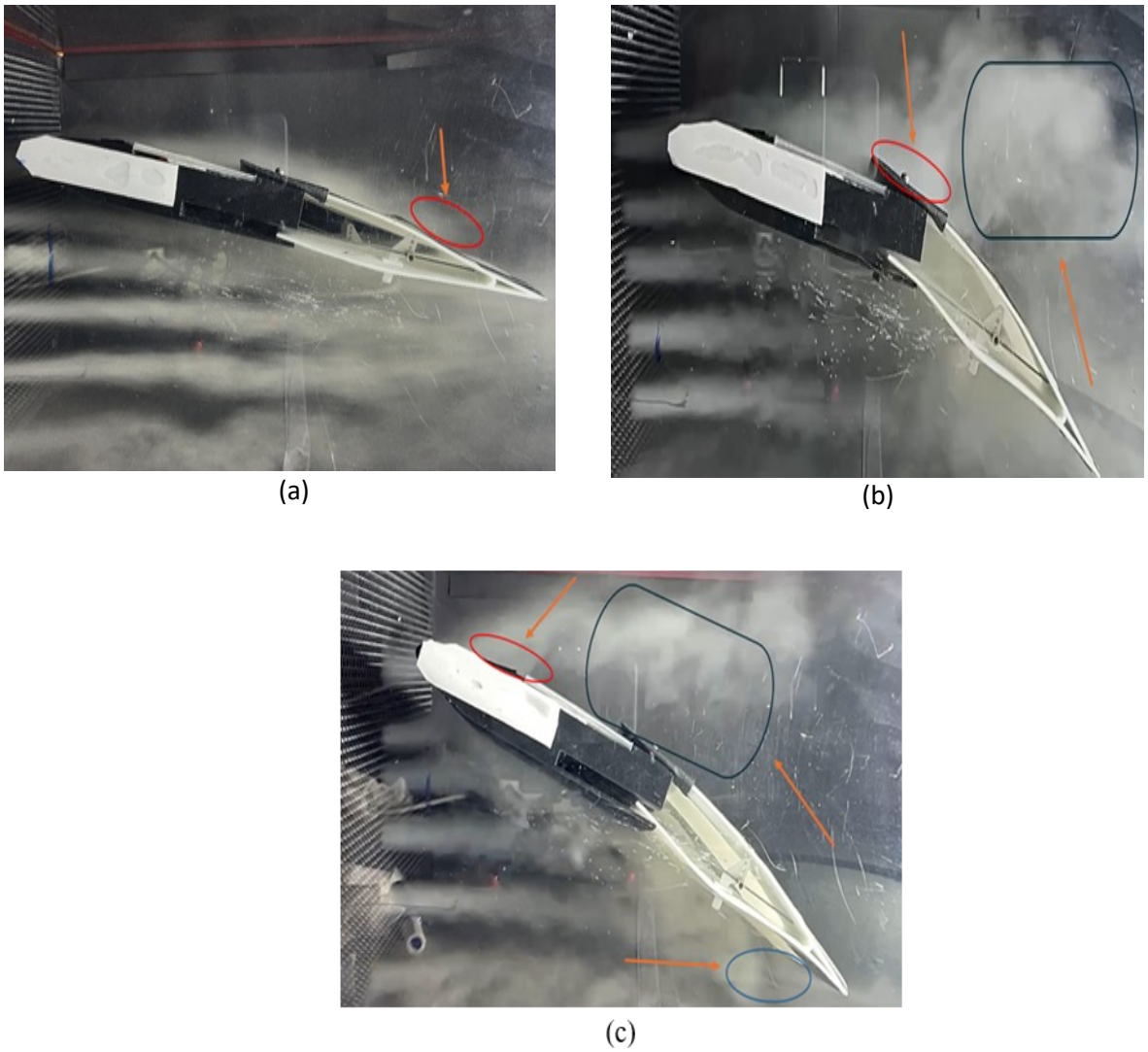

Fig. 7. The flow across the actively cambered airfoil in the wind tunnel at different AOA: (a) 10 degrees, (b) 15 degrees, and (c) 18 degrees retrieved from [23]

The experimental results in Fig. 7 (b), indicating an AOA of 15°, show a definite but delayed flow separation zone ranging from roughly 60% of the chord (x/D = 0.6) to the trailing edge. A small zone of backflow exists, supporting the simulation's prediction of partial separation under these conditions. The SST k-ω model accurately captures unstable separation initiation under moderate cambering, as evidenced by the correlation between experimental smoke lines and vortex roll-up zones and velocity deficits in CFD contours. Fig. 7 (c), at AOA 18°, shows a fully separated flow regime with the separation bubble originating at the leading edge. This discovery complements the modeling results, which similarly showed a total collapse of flow control efficacy at high AOAs as the impact of cambering reduces. The little pressure recovery and early flow detachment seen both experimentally and computationally demonstrate that, above a threshold AOA, cambering alone is unable to minimize separation. Thus, the experimental flow visualization strongly confirms the simulation findings, particularly in terms of separation delay trends, validating the trustworthiness of the numerical model and boundary conditions utilized in this investigation.

Furthermore, in the current experimental setup which is based on qualitative observations measurements such as using smoke visualization in a low speed wind tunnel, this setup helped find and visualize the starting position of the flow separation over the airfoil surface and provided a clear

observation of the airflow behaviour. The airflow pattern and the separation occurred along the airfoil using CFD analysis had helped in confirming the airflow visualization by the wind tunnel. However, in future experimental stages it will include quantitative testing tools such as hot-wire anemometry and a pressure sensor to validate the numerical simulations and quantify the velocity profile and turbulence characteristics. These enhancements will help in collecting of comprehensive flow field data, which will increase the dependability of the CFD validation.

4.2 Time-Averaged Velocity Across the Airfoil

Fig. 8 depicts the time-averaged velocity profiles for four distinct cases: AOA 15° with VGs, AOA 15° cambered, AOA 17° uncambered without VGs, and AOA 17° cambered with VGs. To enable a comparison of flow characteristics under various situations, the velocity is normalized by dividing it by the free-stream velocity (44.32 m/s). To provide a non-dimensional depiction of the spatial velocity distribution, the location is also normalized by dividing by the chord length. The measurements were made 0.08 m from the airfoil surface, which is beyond the boundary layer but sufficiently close to record the aerodynamic effects caused by cambering and VGs. Characteristics of flow attachment, separation, and reattachment may be clearly seen from this optimal measuring position.

Acceleration close to the leading edge causes the velocity to first increase at AOA 15°, as is predicted by standard airfoil flow mechanics. But when the flow moves downstream, the adverse pressure gradient causes the velocity to drop, which leads to slowing and possible separation. The velocity in the VGs scenario (Figure a) increases near x/D = 0.2 and then progressively decreases, as predicted. The velocity loss is less severe, though, since the VGs have generated streamwise vortices, which suggests better boundary layer momentum retention and delayed separation. By encouraging improved momentum mixing, VGs effectively stabilize the boundary layer, as seen by the flow remaining connected throughout the airfoil. On the other hand, a more dramatic drop in velocity is shown in the cambered scenario (Figure b), especially in the area between x/D = 0.6 and x/D = 1.18, where flow separation and backflow effects are evident. This implies that at this AOA, cambering is not enough to stop boundary layer separation. In contrast to the abrupt acceleration seen in the VGs instance, the velocity increases gradually and smoothly close to the trailing edge. This suggests that whereas VGs retain attachment but cause more abrupt velocity fluctuations because of their localized turbulence effects, cambering improves the pressure distribution and results in a more regulated exit flow.

At AOA 17°, flow separation becomes more dominant due to the increased adverse pressure gradient associated with the higher AOA. In the uncambered case without VGs (Figure d), the velocity profile reveals a sharp drop beyond x/D = 0.2, indicating early boundary layer separation and the formation of a large wake region. The steep decline in velocity confirms that the flow loses momentum rapidly, leading to a detached, recirculating region downstream. The nearly flat velocity profile beyond x/D ≈ 0.4 further confirms the presence of a fully separated wake, where the velocity does not recover, signifying a loss of effective lift and a substantial increase in drag. The absence of flow control mechanisms in this case allows separation to dominate, resulting in an unfavorable aerodynamic performance with reduced lift-to-drag efficiency. In contrast, in the cambered case with VGs (Figure c), the velocity profile behaves differently due to the combined influence of cambering and VG-induced turbulence. After x/D = 0.2, velocity still decreases, but the drop is not as steep as in the uncambered case, indicating that cambering plays a significant role in maintaining boundary layer energy. The gradual reduction in velocity suggests that the flow remains partially attached for a longer distance, preventing the formation of an immediate, large separation bubble. The wake region

is also significantly smaller compared to Figure d, confirming that VGs help reattach the flow while cambering adjusts the pressure gradient to maintain a smoother acceleration pattern. Additionally, the wake formation is noticeably delayed, meaning that separation occurs much later than in the uncambered case, resulting in better aerodynamic efficiency. The higher velocity recovery near the trailing edge in Figure c compared to Figure d further indicates that the combination of VGs and cambering successfully mitigates wake expansion and turbulence intensity.

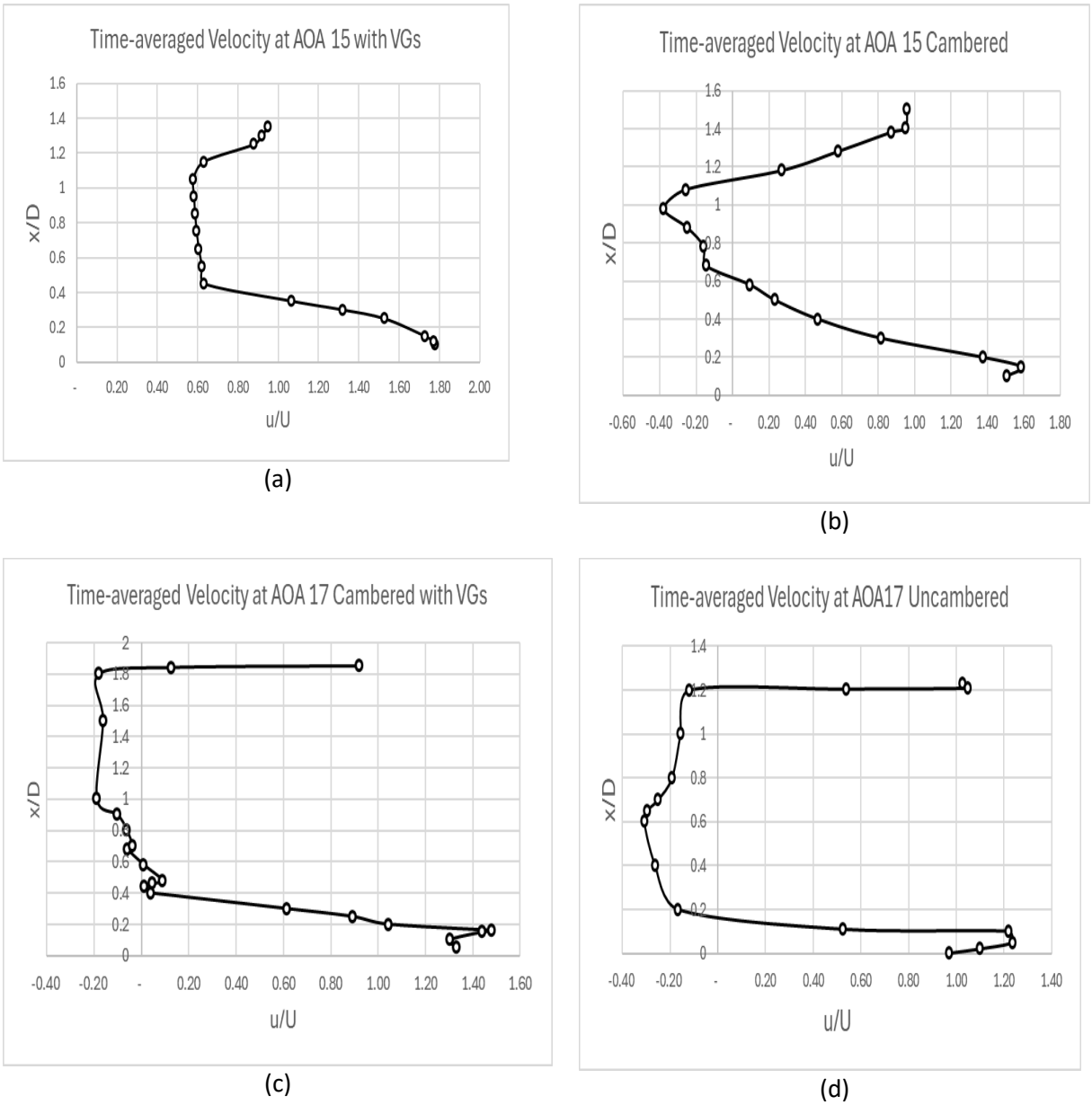

Fig. 8. The normalized time-averaged velocities with respect to the location on the airfoil at: (a) AOA 15 with VGs, (b) AOA 15 with cambered airfoil, (c) AOA 17 cambered with VGs, and (d) AOA 17 uncambered with no VGs.

Turbulent Intensity and Kinetic Energy Budget

Fig. 9 shows the turbulence kinetic energy (TKE) distributions for four aerodynamic configurations: AOA 17° uncambered without VGs (a), AOA 17° cambered with VGs (b), AOA 15° uncambered with VGs (c), and AOA 15° cambered without VGs (d). Shear layer instability, wake production, and separation behaviour are all closely related to TKE, an essential quantity that describes the strength of turbulent oscillations. Zones of substantial velocity gradients are indicated by high TKE areas, which may imply large-scale flow disruptions and powerful vortex shedding. Understanding how VGs and cambering affect turbulence formation, boundary layer attachment, and separation management becomes clearer by comparing these profiles. TKE values were expressed in m^2/s^2, and the turbulence distributions were measured throughout the airfoil chord, normalized by chord length (x/D). The peak TKE values and their locations provide insight into where separation occurs and how flow control techniques modify the turbulence structure.

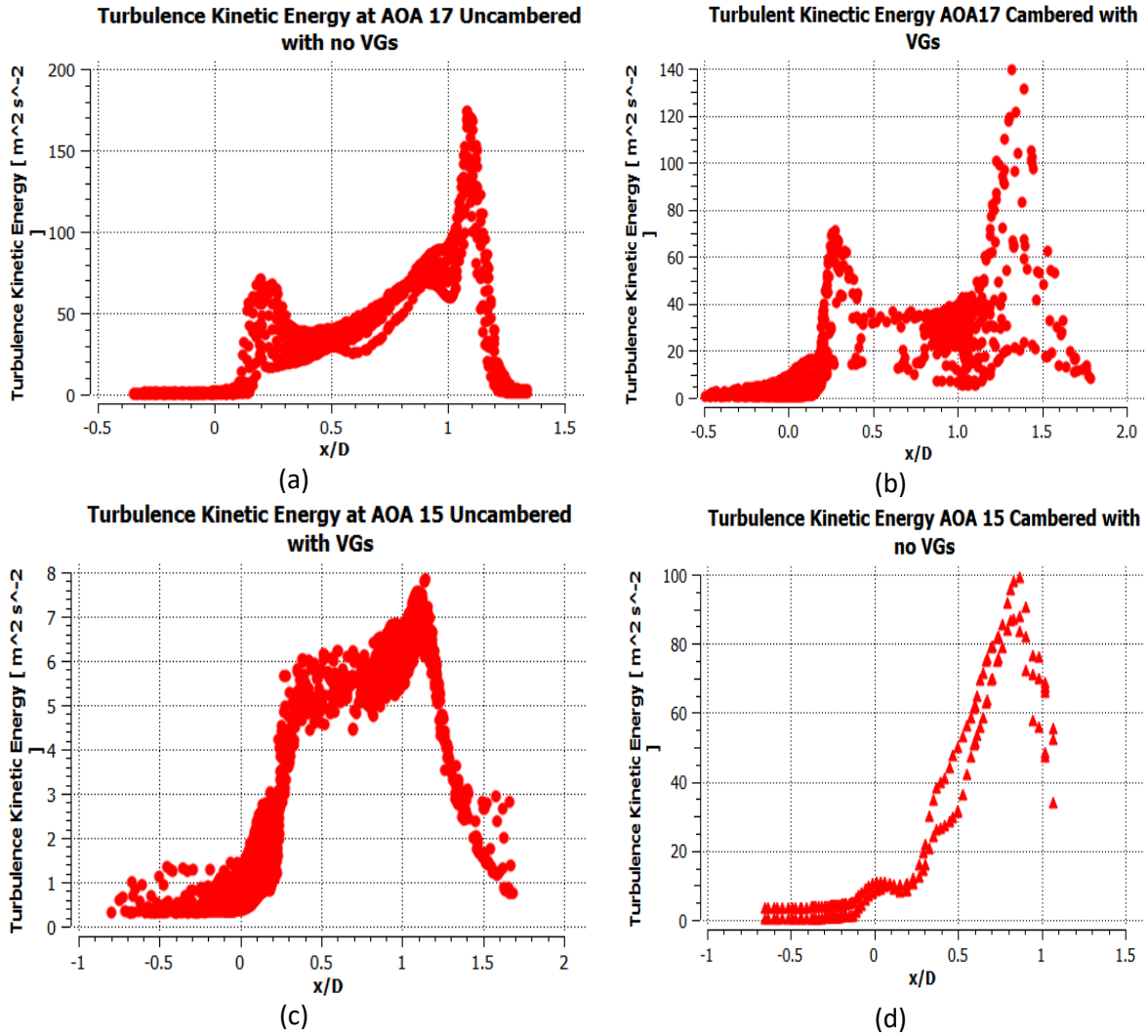

Fig. 9. Turbulence kinetic energies with respect to distance on the airfoil at: (a) AOA 17 uncambered with no VGs, (b) AOA 17 cambered with VGs, (c) AOA 15 uncambered with VGs, and (d) AOA 15 cambered with no VGs.

The function of cambering and VGs in regulating turbulent energy is demonstrated by comparing Figures (a) and (b). Without flow control, TKE peaks at 170 Figure (a) at x/D = 1.2, when wake production and flow separation are at their highest levels. After x/D ≈ 0.5, the TKE profile rises sharply, indicating that the boundary layer cannot tolerate the adverse pressure gradient and separates prematurely. Shear layer instability is shown by the substantial turbulence generation at x/D = 1.2, where the low-momentum separated zone interacts with the high-velocity outer flow, resulting in increased wake turbulence and vortex shedding. Given that increasing drag and lift degradation are closely correlated with strong turbulence, this situation exemplifies the least effective aerodynamic performance. When cambering and VGs are used, TKE drops to a lower high of 140 in Figure (b), indicating an 18% decrease in turbulence intensity. The steady increase in TKE relative to Figure (a) indicates that the flow stays connected for a longer period before running into turbulence. The peak appears farther downstream, suggesting a delayed separation point, in contrast to the uncambered example. According to the numerous smaller turbulence peaks, the VGs assist in maintaining attachment by introducing regulated turbulence sooner in the boundary layer. In the meantime, cambering lessens the severity of separation by adjusting the pressure gradient. The wake zone becomes less chaotic as a result, improving aerodynamic performance and lowering pressure drag.

The effects of VGs and cambering on turbulence formation at a decreased AOA are illustrated in Figures (c) and (d). The maximum TKE stays below 8 in Figure (c) (uncambered with VGs), which is far lower than in any other scenario. The slow increase and decrease in TKE show that VGs are effective at controlling turbulence strength, forming tiny vortices that maintain boundary layer attachment without producing too much turbulence. Strong TKE peaks are absent, indicating that the boundary layer is still under control and has little separation impact. This supports VGs' efficacy at moderate AOAs, when their main function is to avoid detachment rather than to reverse violent separation. On the other hand, the TKE exceeds 100 in Figure (d), which is cambered without VGs, indicating a very unstable boundary layer. Over the chord, the turbulence profile gradually rises, indicating a constant increase in the severity of separation. The cambered example shows turbulence spread across a considerably larger region, especially close to the trailing edge (x/D > 1.0), in contrast to the uncambered VG case, where TKE is concentrated. This implies that although cambering enhances lift performance, the boundary layer is not sufficiently energized by it to sustain full attachment. A more chaotic flow pattern and increased turbulence intensity close to the wake are the results of the lack of controlled turbulence mechanisms like VGs.

The overall TKE for the AOA 15° with VGs example stayed low, below 8, indicating that the boundary layer remained mostly connected with little energy loss from turbulence. But as Fig. 10 illustrates, there are isolated areas of high TKE close to the VGs, where the TKE was 92.4. In order to create a turbulent boundary layer that keeps momentum close to the wall and avoids early flow separation, a localized increase in turbulent energy is necessary. The VGs successfully create streamwise vortices, which improve momentum mixing in the boundary layer, as indicated by the high TKE values close to the VG position. By improving the boundary layer's resistance to the adverse pressure gradient, these vortices postpone or completely prevent separation. The figure also shows concentrated turbulence bands near the VG wake, highlighting how the vortices propagate downstream. Beyond these regions, the TKE rapidly dissipates, ensuring that the flow remains mostly stable and attached across the airfoil surface. This confirms that VGs achieve their intended function—localized turbulence generation—without excessively increasing overall drag, making them an efficient flow control solution for AOA 15°.

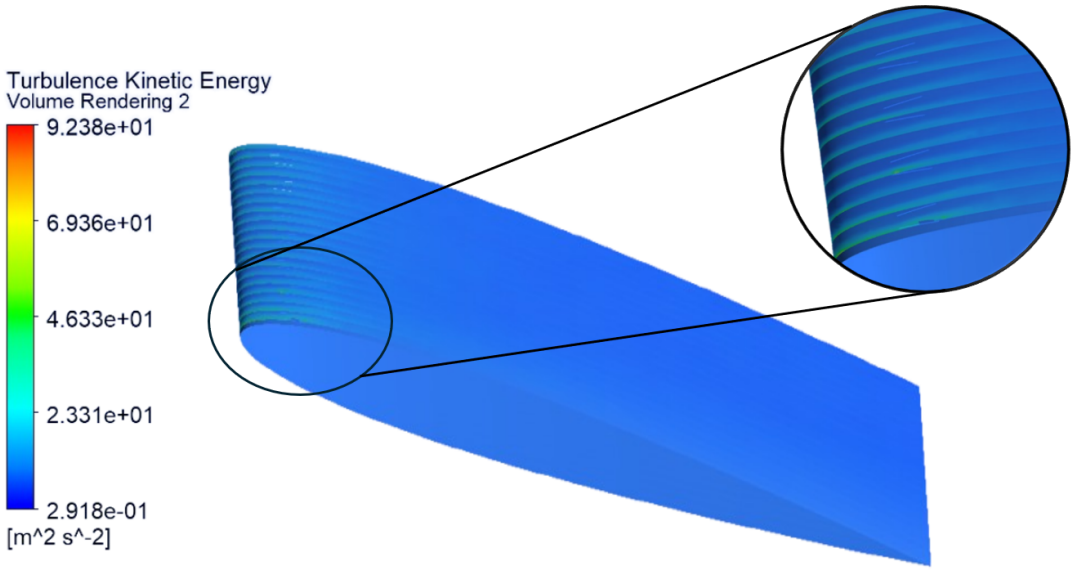

Fig. 10. The turbulence kinetic energy near the VGs.

4.3 Drag Penalties

As shown in Fig. 11, at low AOA (0°–6°), cambering demonstrates a more pronounced positive influence on aerodynamic efficiency compared to the addition of VGs. Increasing the camber by 5% at 70% chord enhances the airfoil curvature, strengthens circulation, and produces a more favorable pressure distribution, resulting in higher lift-to-drag ratios (CL/CD) with minimal drag penalties. In this regime, flow separation is minimal, and the boundary layer remains largely attached; therefore, the performance gains are primarily driven by the additional lift generated through camber modification. VGs, in contrast, provide limited benefit at these conditions as there is little separated flow to re-energize, and their presence may contribute to parasitic drag. Consequently, the cambered configurations outperform the uncambered ones in this range, with peak efficiency achieved by the cambered configuration without VGs at moderately low angles of attack, and only marginal differences observed when VGs are added.

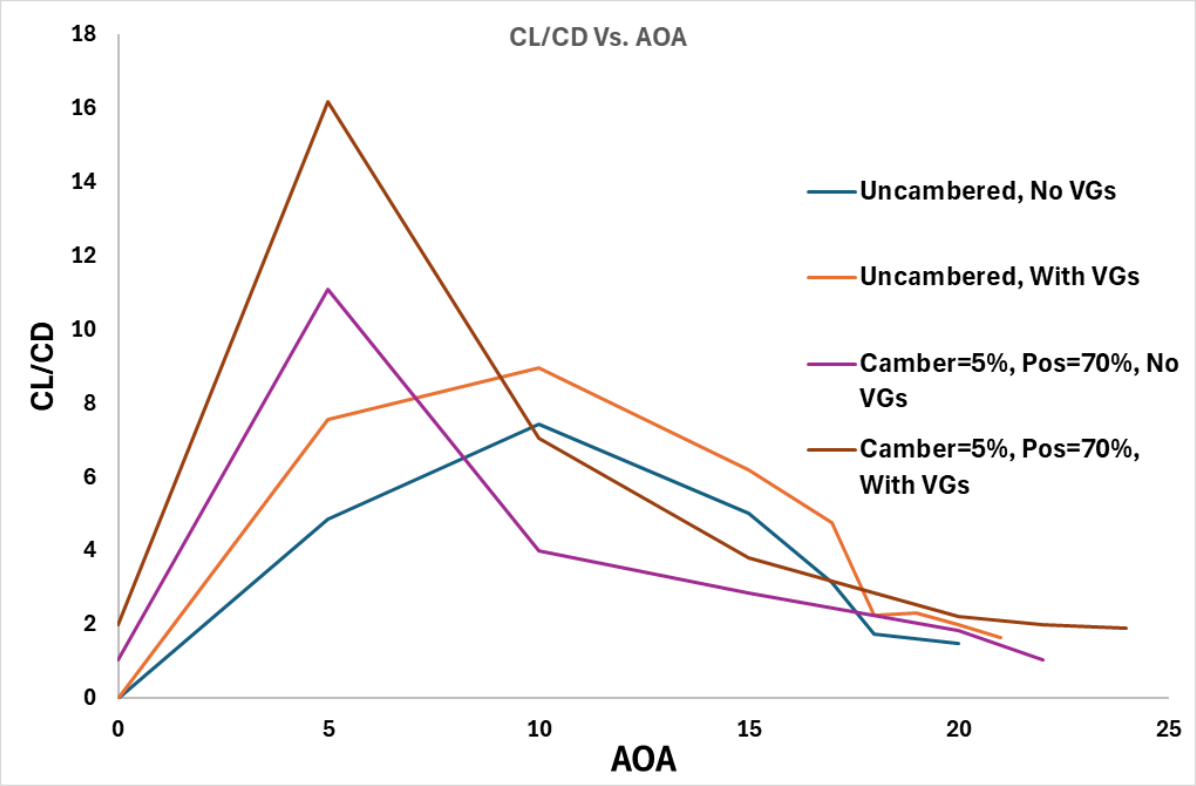

Fig. 11. Lift to drag coefficient concerning different angles of attack and airfoil modifications.

At higher AOA (above approximately 8°), VGs become more effective, while the relative benefits of cambering decrease. As the adverse pressure gradient intensifies, the boundary layer thickens and flow separation occurs earlier, particularly on cambered airfoils where curvature is more pronounced. In this range, the uncambered configuration with VGs achieves the highest CL/CD values, as the devices generate streamwise vortices that energize the near-wall flow and delay separation further aft along the chord. While VGs on cambered airfoils still improve performance compared to cambered without VGs, the increased form drag and earlier separation associated with higher camber limit their effectiveness. These results suggest that for morphing wing applications, greater camber is advantageous at AOA, whereas reduced camber combined with VGs is preferable at high angles of attack to sustain attached flow and maintain aerodynamic efficiency. This supports the conclusions from previous sections, highlighting the behaviour of the integrated modifications based on drag penalties.

5. Conclusion and Recommendations

5.1 Main Conclusions and Contributions

This study systematically investigated the aerodynamic performance and turbulence characteristics of a NACA 0009 airfoil under different flow control strategies, specifically focusing on camber morphing and VGs across a range of AOA. The analysis combined CFD simulations with experimental validation to examine velocity fields, turbulence behaviour, and flow separation dynamics. Results revealed that VGs effectively delay flow separation by energizing the boundary layer through the introduction of streamwise vortices, while camber morphing contributes by

optimizing pressure distribution. While both strategies improve flow stability, VGs were found to be more effective at higher AOAs, particularly in maintaining boundary layer attachment. On the other hand, cambering alone was insufficient to prevent separation under more aggressive flow conditions. The combined use of cambering and VGs showed a clear synergistic effect, improving both flow control and aerodynamic stability. Quantitatively, the system was analyzed in different stages across various comparisons and parametric tests, and the obtained results can be summarized as follows:

- At AOA 17° without cambering or VGs, severe separation occurred around x/D ≈ 1.2, and TKE peaked at 170 m^2/s^2, indicating strong wake-induced turbulence and aerodynamic inefficiency.
- When VGs were added along with cambering, TKE was reduced to 140 m^2/s^2, demonstrating an 18% improvement in flow stability and separation delay.
- At AOA 15° uncambered with VGs, the TKE remained below 8 m^2/s^2, highlighting effective boundary layer control and minimal turbulence generation.
- in the cambered case without VGs, the TKE reached 100 m^2/s^2, confirming that cambering alone was insufficient to fully prevent separation, particularly at higher AOAs.
- The localized TKE near the VGs peaked at 92.4, confirming their role in initiating controlled turbulence to sustain boundary layer attachment.

5.2 Future Work and Recommendations

Future improvement will focus on optimizing the size, spacing, number, and positioning distance of VGs from the leading edge. This will enhance aerodynamic efficiency while decreasing turbulence-induced drag. The Taguchi technique offers an effective approach to finding optimal configurations while lowering computational costs. It employs orthogonal arrays to systematically analyze these factors and quantify the contribution of each of them. This technique ensures that the optimum VG positioning and dimensions are chosen to maintain boundary layer attachment with the least amount of energy loss by experimenting with different combinations. It, moreover, quantifies the contribution of each factor, assisting researchers in design of experiments and decision making. Furthermore, the airfoil profile and AOA can also be introduced as variable factors within the Taguchi design to evaluate their influence on VG effectiveness and overall flow control. By including these aerodynamic parameters alongside VG geometry and placement, the experimental matrix becomes more comprehensive, allowing for deeper insight into the interaction between airfoil shape, operational conditions, and flow control strategies. This would not only broaden the applicability of the results but also help identify robust configurations that perform well across a range of realistic UAV or aircraft scenarios.

References

[1] Ye C, Wang Y, An D, Chen J, Yan H, Zheng Y, et al. Study of Hydrofoil Boundary Layer Prediction with Two Correlation-Based Transition Models. J Mar Sci Eng 2024;12:1965. https://doi.org/10.3390/jmse12111965.

[2] Öksüz S, Usta O, Celik F. Investigation of numerical solution approaches for the cavitating flow analysis of twisted hydrofoils. Ocean Engineering 2024;312:119198. https://doi.org/10.1016/j.oceaneng.2024.119198.

[3] Ausoni P, Farhat M, Avellan F. Cavitation in Ka´rma´n Vortex Shedding From 2D Hydrofoil: Wall Roughness Effects. Volume 2: Fora, Parts A and B, ASMEDC; 2007, p. 489–95. https://doi.org/10.1115/FEDSM2007-37562.

[4] Xie N, Tang Y, Liu Y. High-fidelity numerical simulation of unsteady cavitating flow around a hydrofoil. Journal of Hydrodynamics 2023;35:1–16. https://doi.org/10.1007/s42241-023-0014-2.

[5] Jini Raj R, Rose J BR. Influence of bioinspired morphing on the flow field characteristics of UAV wings at low Reynolds number. Proc Inst Mech Eng G J Aerosp Eng 2024;238:1503–33. https://doi.org/10.1177/09544100241274864.

[6] Kaya F, Akbıyık H. Investigation of the effects of bioinspired vortex generators on aerodynamic performance of a NACA0015 airfoil. Bioinspir Biomim 2025;20:016030. https://doi.org/10.1088/1748-3190/ada1bc.

[7] Hollenbeck AC, Beachy AJ, Grandhi R V., Pankonien AM. Data-Driven Sparse Sensor Placement Optimization on Wings for Flight-By-Feel: Bioinspired Approach and Application. Biomimetics 2024;9:631. https://doi.org/10.3390/biomimetics9100631.

[8] Tang D, Liu D, Zhu H, Huang X, Fan Z, Lei M. Shape reconstructions and morphing kinematics of an eagle during perching manoeuvres*. Chinese Physics B 2020;29:024703. https://doi.org/10.1088/1674-1056/ab610a.

[9] Wei Z, Wang S, Farris S, Chennuri N, Wang N, Shinsato S, et al. Towards silent and efficient flight by combining bioinspired owl feather serrations with cicada wing geometry. Nat Commun 2024;15:4337. https://doi.org/10.1038/s41467-024-48454-3.

[10] Joseph J, A. S, Sridhar S. Experimental and numerical analysis of humpback whale inspired tubercles on swept wings. Aircraft Engineering and Aerospace Technology 2022;94:1577–92. https://doi.org/10.1108/AEAT-04-2021-0114.

[11] Yu Y, Lu Q, Zhang B. Reinforcement learning based recovery flight control for flapping-wing micro-aerial vehicles under extreme attitudes. Int J Adv Robot Syst 2025;22. https://doi.org/10.1177/17298806241303290.

[12] Dol SS, Hamdan H, Ahmad KA. Numerical and Experimental Analysis of Multiphase Flows in Subsea Electric Submersible Pumps. Journal of Advanced Research in Experimental Fluid Mechanics and Heat Transfer 2025;20:68–90. https://doi.org/10.37934/arefmht.20.1.6890.

[13] Clements D, Djidjeli K. Periodic morphing of a NACA6409 aerofoil in ground effect, its wake mechanisms and thrust generation. The Aeronautical Journal 2024;128:2924–44. https://doi.org/10.1017/aer.2024.80.

[14] Marciniuk M, Piskur P, Kiszkowiak Ł, Malicki Ł, Sibilski K, Strzelecka K, et al. Aerodynamic Analysis of Variable Camber-Morphing Airfoils with Substantial Camber Deflections. Energies (Basel) 2024;17:1801. https://doi.org/10.3390/en17081801.

[15] Feng C, Chen S, Yuan W, Li Z, Gao Z. A wide-speed-range aerodynamic configuration by adopting wave-riding-strake wing. Acta Astronaut 2023;202:442–52. https://doi.org/10.1016/j.actaastro.2022.11.010.

[16] Nikkhoo A, Esmaeili A. Geometrical parameters effect on aerodynamic performance of infinite tubercle leading edge wings. Energy Sources, Part A: Recovery, Utilization, and Environmental Effects 2024;46:13596–615. https://doi.org/10.1080/15567036.2024.2406388.

[17] Akhter MdZ, Ali AR, Omar FK. Aerodynamics of a three-dimensional bionic morphing flap. Sustainable Energy Technologies and Assessments 2022;52:102286. https://doi.org/10.1016/j.seta.2022.102286.

[18] Shao H, Li D, Kan Z, Li H, Yuan D, Xiang J. Influence of wing camber on aerodynamic performance of flapping wing rotor. Aerosp Sci Technol 2021;113:106732. https://doi.org/10.1016/j.ast.2021.106732.

[19] Kooshartoyo M, Yohana E, Zuhdi Pane I. Visualization Analysis of Flow with Smoke on Airfoils and Flaps. Journal of Advanced Research in Experimental Fluid Mechanics and Heat Transfer Journal Homepage 2025;21:70–6. https://doi.org/10.37934/arefmht.21.1.7076.

[20] De Tavernier D, Ferreira C, Viré A, LeBlanc B, Bernardy S. Controlling dynamic stall using vortex generators on a wind turbine airfoil. Renew Energy 2021;172:1194–211. https://doi.org/10.1016/J.RENENE.2021.03.019.

[21] Lin JC. Review of research on low-profile vortex generators to control boundary-layer separation. Progress in Aerospace Sciences 2002;38:389–420. https://doi.org/10.1016/S0376-0421(02)00010-6.

[22] Algan M, Seyhan M, Sarioğlu M. Effect of aero-shaped vortex generators on NACA 4415 airfoil. Ocean Engineering 2024;291:116482. https://doi.org/10.1016/J.OCEANENG.2023.116482.

[23] Dol SS, Pagaling JR, Almansoori D, Hamdan H, Ahmad KA. Enhanced Aerodynamic Performance of NACA 0009 Morphing Airfoil: A Study on Camber Morphing and Vortex Generators. Journal of Advanced Research in Experimental Fluid Mechanics and Heat Transfer 2025;20:41–67. https://doi.org/10.37934/arefmht.20.1.4167.

[24] Zhao Z, Jiang R, Feng J, Liu H, Wang T, Shen W, et al. Researches on vortex generators applied to wind turbines: A review. Ocean Engineering 2022;253:111266. https://doi.org/10.1016/J.OCEANENG.2022.111266.

[25] Han Z, Li J, Chen Z, Liu W, Xu Z. Particulate fouling characteristics of wing vortex generator under pulsating flow. International Journal of Thermal Sciences 2025;210:109646. https://doi.org/10.1016/J.IJTHERMALSCI.2024.109646.

[26] Das AK, Hiremath SS. Multi-objective optimization of a novel butterfly-wing vortex generator fabricated in a rectangular microchannel based on CFD and NSGA-II genetic algorithm. Appl Therm Eng 2023;234:121187. https://doi.org/10.1016/J.APPLTHERMALENG.2023.121187.

[27] Godard G, Stanislas M. Control of a decelerating boundary layer. Part 1: Optimization of passive vortex generators. Aerosp Sci Technol 2006;10:181–91. https://doi.org/10.1016/J.AST.2005.11.007.

[28] Younoussi S, Ettaouil A. Calibration method of the k-ω SST turbulence model for wind turbine performance prediction near stall condition. Heliyon 2024;10:e24048. https://doi.org/10.1016/J.HELIYON.2024.E24048.

[29] Townsend JF, Xu G, Jin Y. Roughness constant selection for atmospheric boundary layer simulations using a k-ω SST turbulence model within a commercial CFD solver. Advances in Wind Engineering 2024;1:100005. https://doi.org/10.1016/J.AWE.2024.100005.

[30] Kim KW, Paik KJ, Lee JH, Song SS, Atlar M, Demirel YK. A study on the efficient numerical analysis for the prediction of full-scale propeller performance using CFD. Ocean Engineering 2021;240:109931. https://doi.org/10.1016/J.OCEANENG.2021.109931.